Preprints of the 21st IFAC World Congress (Virtual)
Berlin, Germany, July 12-17, 2020

A Performance Comparison of PLL Implementations in Low-Inertia Power Systems Using an Observer-Based Framework

Juan G. Rueda-Escobedo * **Shiqing Tang** ** **Johannes Schiffer** *

* *Fachgebiet Regelungssysteme und Netzleittechnik, Brandenburgische Technische Universität Cottbus - Senftenberg (e-mail:{ruedaesc,schiffer}@b-tu.de)*
** *University of Shanghai for Science and Technology(e-mail:penny.tang@fim-tec.com)*

Abstract: Phase-locked loop (PLL) implementations are critical components for the control and operation of grid-connected converters. Hence, they have to exhibit a highly reliable behavior under a wide range of operating conditions. Available implementations and performance analyses mainly focus on the impact of unbalances and harmonics. However, in converter-dominated low-inertia power systems an additional important type of perturbation will arise from fast variations in the grid frequency. Motivated by this, we show that the structure of several popular PLL implementations is closely related to that of high-gain observers and, by using this framework, provide a tuning criterion for the PLL gains that mitigates the impact of the rate of change of the frequency (RoCoF) on the estimation performance. This criterion is then used to conduct a numerical comparison of four popular PLL implementations under three distorted conditions: unbalances, harmonics and frequency variations.

Keywords: Phase-locked loop implementations; Frequency estimation; High-gain observers; Electric power systems; Low-inertia systems; Inverter-based applications

1. INTRODUCTION

Future power systems (PS) are expected to be dominated by renewable energy generation (Tielens and Hertem, 2016). Since most renewable energy generators are interfaced to the grid with power electronic converters instead of synchronous machines, the overall system inertia will be significantly reduced leading to *low-inertia PS* (Ørum et al., 2015; Milano et al., 2018). Low-inertia systems are expected to possess highly volatile system dynamics and, thus, exhibit more often events, during which the grid frequency significantly deviates from its nominal value (Tielens and Hertem, 2016). This implies that the availability of an accurate and reliable estimation of the frequency becomes increasingly important, not only for the classical task of synchronizing converter-interfaced generation units to the grid, but also to deliver primary and enhanced frequency control with converter-interfaced generators (Ørum et al., 2015; Milano et al., 2018).

The most prominent method for grid-synchronization in grid-connected converter applications are phase-locked loop (PLL) implementations (Rocabert et al., 2012; Teodorescu et al., 2011). In addition to estimating the phase angle at the coupling point to the grid, these implementations can also provide an estimate of the grid frequency (Milano et al., 2018). The original PLL implementations are designed assuming a constant frequency and undistorted measurements. Over the past years, different modification and methodologies have been proposed to address the presence of unbalances and harmonics in the measured electrical signals (Teodorescu et al., 2011).

Yet, in low-inertia systems another important source of perturbations are faster and more pronounced variations of the frequency itself (Tielens and Hertem, 2016). This fact has only very recently been recognized, but has already motivated a series of investigations on the effect such frequency variations have on the PLL and the overall system performance (Göksu et al., 2014; Bizzarri et al., 2018; Rueda-Escobedo et al., 2019). In particular, the recent studies (Ma et al., 2017; Khan et al., 2018; Poolla et al., 2019) have shown that the performance of the PLL is a key factor for the quality of frequency support, which could be provided by converter-based generation units. Given the increasingly prominent role of PLLs in power system applications, we present the next three main contributions:

1. It is shown that the canonical structure of popular PLL implementations is closely related to that of a high-gain observer, in which variations in the frequency can be interpreted as perturbations.
2. Based on the above observation, a tuning criterion for the PLL gains, aimed at attenuating the effect of frequency variations is presented. This criterion is derived by relating the PLL gains to those of a high-gain observer (Besançon, 2007; Khalil, 2017) and following an input-to-state (ISS) stability approach (Besançon, 2007, Theo. 6). In contrast to available tuning methods based on small gain analysis and frequency response (Freijedo et al., 2009; Golestan et al., 2013), the non-linearities present in the PLL are explicitly considered and conditions that guarantee a bounded estimation error are provided.
3. Using a high gain may amplify the effect of other disturbances. To evaluate this phenomenon in the PLL case, the performance of four popular PLL implementations, tuned with the proposed criterion, is evaluated numerically for different gains and under three distorted conditions: unbalances, harmonics

and frequency variations. Thereby, the $\mathcal{L}_2$ and $\mathcal{L}_\infty$ norms of the frequency estimation error are used as performance metrics.

The organization of the paper is as follows. In Section 2, usual representations of AC signals are reviewed. In Section 3, the connection between PLL implementations and observers is established and the main result is derived. In Section 4, several popular PLL implementations are reviewed. In Section 5, the results of the numerical case study are provided. Finally, the proof of the main result is given in Appendix A.

Notation: $\mathbb{Z}$ denotes the set of integer numbers, $\mathbb{R}$ the set of real numbers, $\mathbb{R}_{\geq 0}$ the interval $[0,\infty)$, $\mathbb{R}^n$ the real n-dimensional Euclidean space and $\mathbb{R}^{n\times m}$ the set of $n\times m$ real matrices. Also, $\mathbf{I}_n \in \mathbb{R}^{n\times n}$ denotes the identity matrix. For symmetric matrices $A\in\mathbb{R}^{n\times n}$ and $B\in\mathbb{R}^{n\times n}$, $A>B$ ($A\geq B$) means that $A-B$ is positive (semi)definite, and $\lambda_{\min}(A)$ and $\lambda_{\max}(A)$ denote the smallest and the largest eigenvalues of A. For $v\in\mathbb{R}^n$, $\|v\|=(v^\top v)^{1/2}$ denotes the Euclidean norm and for $B\in\mathbb{R}^{m\times n}$, $\|B\|$ denotes the induced Euclidean norm of B, defined as $\sup_{\|x\|=1}\|Bx\|$. Finally, $\mathbf{e}$ denotes the Euler.

2. REPRESENTATION OF THREE-PHASE AC SIGNALS

In AC PS, physical variables such as currents and voltages are modeled as sinusoidal signals. A particular model is the symmetric three-phase AC signals model. A symmetric three-phase signal $v_{abc}(t)\in\mathbb{R}^3$ is characterized by its phase $\phi(t)\in\mathbb{R}_{\geq 0}$, its amplitude $A(t)\in\mathbb{R}_{\geq 0}$ and the relationship (Schiffer et al., 2016):

$$v_{abc}(t)=\begin{bmatrix} v_a(t)\\ v_b(t)\\ v_c(t)\end{bmatrix}=A(t)\begin{bmatrix}\cos(\phi(t))\\ \cos\left(\phi(t)-\frac{2\pi}{3}\right)\\ \cos\left(\phi(t)+\frac{2\pi}{3}\right)\end{bmatrix}. \tag{1}$$

The signal's frequency is denoted by $\omega(t)$ and defined as $\dot{\phi}(t)=\omega(t)$. The instantaneous frequency $\omega(t)$ is common to all components of $v_{abc}(t)$ in (1). The signal $v_{abc}(t)$ can be equivalently described in a coordinate system contained in a plane. The signal's components in this plane are called $\alpha\beta 0$-components (Teodorescu et al., 2011), and can be obtained by using the Clarke transformation, denoted by $T_{\alpha\beta 0}$, and whose definition can be found in (Teodorescu et al., 2011, Appx. A). When the Clarke transformation is applied to the signal $v_{abc}(t)$, one obtains the following structure:

$$v_{\alpha\beta 0}(t)=T_{\alpha\beta 0}v_{abc}(t)=A(t)\begin{bmatrix}\cos(\phi(t))\\ \sin(\phi(t))\\ 0\end{bmatrix}.$$

Another convenient coordinate representation for symmetric AC signals are the $dq0-$coordinates, which are obtained using the Park transformation. Consider an auxiliary angle $\hat{\phi}(t)$. The Park transformation matrix is defined as (Teodorescu et al., 2011):

$$T_{dq0}\left(\hat{\phi}(t)\right):=\begin{bmatrix}\cos(\hat{\phi}(t)) & \sin(\hat{\phi}(t)) & 0\\ -\sin(\hat{\phi}(t)) & \cos(\hat{\phi}(t)) & 0\\ 0 & 0 & 1\end{bmatrix}. \tag{2}$$

By using the Park transformation, the signal $v_{\alpha\beta 0}(t)$ results in:

$$v_{dq0}(t)=T_{dq0}\left(\hat{\phi}(t)\right)v_{\alpha\beta 0}(t)=A(t)\begin{bmatrix}\cos(\hat{\phi}(t)-\phi(t))\\ -\sin(\hat{\phi}(t)-\phi(t))\\ 0\end{bmatrix}.$$

The importance of this latter coordinates' choice lies in the fact that the second component of $v_{dq0}(t)$, i.e., $v_q(t)=-A(t)\sin(\hat{\phi}(t)-\phi(t))$, provides direct information about the difference between $\phi(t)$ and $\hat{\phi}(t)$. Note that for $\hat{\phi}(t)=\phi(t)$ (modulo 2π) the second and the third components of $v_{dq0}(t)$ are zero, while the first one corresponds to the signal's amplitude. These two observations are exploited by PLL implementations to estimate the signal's phase and frequency.

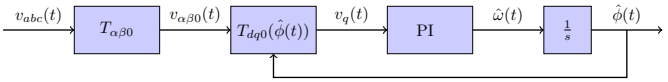

Fig. 1. Block diagram of the SRF-PLL.

Remark 1. The signal $v_{dq0(t)}$ can be made independent of the amplitude $A(t)>0$ if the signal $v_{\alpha\beta 0}(t)$ is normalized before applying the Park transformation.

3. AN OBSERVER FRAMEWORK FOR THE STUDY OF THE SYNCHRONOUS REFERENCE FRAME PLL

3.1 The Synchronous Reference Frame PLL

The synchronous reference frame PLL (SRF-PLL) is by far the most common PLL implementation (Teodorescu et al., 2011). Its design assumes that the measured signal $v_{abc}(t)$ is symmetric and then takes advantage of the structure of symmetric signals to estimate the phase and frequency of $v_{abc}(t)$. To do so, it generates an estimate of the signal's phase $\hat{\phi}(t)$ which is then used as the auxiliary angle of the Park transformation (2), yielding

$$v_q(t)=-A(t)\sin(\hat{\phi}(t)-\phi(t)). \tag{3}$$

For $\hat{\phi}(t)-\phi(t)\in[-\pi/2,\pi/2]$, $v_q(t)$ can be approximated by $v_q(t)\approx -A(t)(\hat{\phi}(t)-\phi(t))$. Hence, to correct the phase, $v_q(t)$ is used as input to a PI control that in turn generates an estimate of the signal's frequency $\hat{\omega}(t)$:

$$\dot{\hat{\phi}}(t)=\hat{\omega}(t)=k_p v_q(t)+k_i\int_{t_0}^{t} v_q\left(\sigma\right)\mathrm{d}\sigma. \tag{4}$$

The estimate $\hat{\omega}(t)$ is then integrated to update the phase estimate $\hat{\phi}(t)$. The closed-loop is obtained by a non-linear feedback of $\hat{\phi}(t)$ via the Park transformation, see (3). The block diagram of this estimation scheme is shown in Figure 1.

3.2 The Synchronous Reference Frame PLL as an Observer

A closer inspection of (4) reveals that the information provided by the Park transformation, i.e., (3), is used to regulate the phase error to zero. That is, the estimation problem is treated as if it was a standard control problem. However, the direct use of the PI controller has the disadvantage of introducing a direct dependency of $v_q(t)$ on the estimate $\hat{\omega}(t)$. This implies that any disturbance corrupting $v_q(t)$ is amplified by the gain k_p, thus deteriorating the estimation quality. Therefore, instead of using directly the PI controller to correct the phase, we propose to interpret the PLL tuning problem as the design of an observer for the phase and the frequency taking as measurement $v_q(t)$, which is a non-linear function of the phase error. As is shown next, this leads to an observer with the same internal dynamics as that of the PI control (4), but with a redefined frequency estimate. In the sequel, for the sake of simplicity, it is assumed that $v_{\alpha\beta 0}(t)$ is normalized before being used in the Park transformation. This renders $v_q(t)$ independent of the signal amplitude, i.e., $v_q(t)=-\sin(\hat{\phi}(t)-\phi(t))$. Now, the observation problem can be formulated by first recognizing that the dynamics of the phase $\phi(t)$ and the frequency $\omega(t)$ correspond to a double integrator of the form

$$\dot{x}(t)=A_0x(t)+b\zeta(t), \tag{5}$$
$$A_0=\begin{bmatrix}0 & 1\\ 0 & 0\end{bmatrix}, b=\begin{bmatrix}0\\ 1\end{bmatrix},$$

with $x^\top(t)=[\phi(t),\omega(t)]$ and where $\zeta(t)=\dot{\omega}(t)\in\mathbb{R}$ represents the RoCoF, which acts as a disturbance.
Next, the PI control in (4) can be interpreted as an observer for (5) by only associating the integral term to the frequency estimate $\hat{\omega}(t)$, instead of the proportional and the integral terms together. Then, the PI dynamics results in

$$\begin{aligned}\dot{\hat{x}}(t)&=A_0\hat{x}(t)+Kv_q(t),\\ K^\top&=\begin{bmatrix}k_p & k_i\end{bmatrix},\end{aligned}\tag{6}$$

with $\hat{x}^\top(t)=[\hat{\phi}(t),\hat{\omega}(t)]$ and A_0 given in (5). Clearly, the dynamics in (6) is a copy of the one in (5) with an additional feedback term of the phase error $v_q(t)$. Now, define the observation error as

$$\tilde{x}^\top(t)=[\tilde{x}_1(t),\tilde{x}_2(t)]=[\hat{\phi}(t)-\phi(t),\hat{\omega}(t)-\omega(t)].$$

By using this notation, $v_q(t)$ corresponds to $-\sin(\tilde{x}_1(t))$. With $C_0=[1,0]$, the error dynamics induced by the PI control then results in

$$\begin{aligned}\dot{\tilde{x}}(t)&=\big(A_0-KC_0\big)\chi(\tilde{x}(t))-b\zeta(t),\\ \chi^\top(\tilde{x}(t))&=\begin{bmatrix}\sin(\tilde{x}_1(t)) & \tilde{x}_2(t)\end{bmatrix}.\end{aligned}\tag{7}$$

In (7), A_0 represents the system matrix, K plays the role of the observer gain and $\sin(\tilde{x}_1(t))$ is the error measurement obtained from the Park transformation, see (3). Note also that the pair (A_0,C_0) is observable. Thus, the eigenvalues of the matrix $A=A_0-KC_0$ can be assigned with K. In particular, for $k_p>0$ and $k_i>0$, the matrix A is Hurwitz.
Clearly, (7) resembles the error dynamics induced by a Luenberger observer. This similarity intuitively suggests to design the gain K as if (6) was a linear observer. One may then expect to obtain similar properties to the linear case, at least, locally. This idea is exploited in Section 3.3.

3.3 High-Gain Design for the Synchronous Reference Frame PLL

From (7), it can be observed that the error dynamics is perturbed by the RoCoF $\zeta(t)$, which appears as an additive disturbance. A class of observers capable of attenuating this kind of disturbances are high-gain observers (Besançon, 2007; Khalil, 2017). One particularity of these observers is that their gains only depend on a single tuning parameter. Moreover, increasing the magnitude of this parameter is is directly related to a reduction of the ultimate bound of the observer error. In this section it is demonstrated that by selecting the gains k_p and k_i in a particular manner, the main properties of high-gain observers can be locally mirrored into the SRF-PLL (7). Compared to existing approaches (Freijedo et al., 2009; Golestan et al., 2013) based on small gain analysis, this yields a rigorous and intuitive tuning procedure for PLLs in a nonlinear setting. Following (Besançon, 2007; Khalil, 2017), we propose to choose the PI gains as

$$\begin{aligned}p(s)&=s^2+h_0s+h_1,\\ k_p=Lh_0>0,&\quad k_i=L^2h_1>0,\end{aligned}\tag{8}$$

with $p(s)$ being a Hurwitz polynomial and where $L>0$ represents the abovementioned, single tuning parameter.
In order to analyze the effect of this choice, let us first briefly discuss the unperturbed case. For $\zeta(t)=0$, the error system (7) has multiple equilibria due to the periodicity of the term $\sin(\tilde{x}_1(t))$. The equilibrium set is described by $\mathcal{S}\cup\mathcal{U}$ with

$$\begin{aligned}\mathcal{S}&=\{(\tilde{x}_1,\tilde{x}_2)\in\mathbb{R}^2,n\in\mathbb{Z}|\tilde{x}_1=2n\pi,\tilde{x}_2=0\},\\ \mathcal{U}&=\{(\tilde{x}_1,\tilde{x}_2)\in\mathbb{R}^2,n\in\mathbb{Z}|\tilde{x}_1=(2n+1)\pi,\tilde{x}_2=0\}.\end{aligned}\tag{9}$$

The stability of the points in $\mathcal{S}$ and $\mathcal{U}$ can be investigated by linearizing the error system (7) around these points. This shows that the points in $\mathcal{S}$ are locally exponentially stable for positive gains, and, under the same circumstances, the points in $\mathcal{U}$ result unstable. Additionally, by using techniques based on invariance like principles (Abramovitch, 1990; Rantzer, 2001), almost global stability of the points in $\mathcal{S}$ can be concluded. However, in the perturbed case these methods are not applicable. Therefore, we instead pursue an ISS-analysis for the case $\zeta(t)\neq0$, which also is of higher practical relevance.
In order to assess robustness of the PLL implementation (7) with respect to the RoCoF, it is of interest to assert if all trajectories starting close to points in $\mathcal{S}$ will remain bounded and how this bound is affected by the choice of the gains k_p and k_i. To this end, we assume a uniformly bounded RoCoF, i.e., $|\zeta(t)|\leq\bar{\zeta}$, for some constant $\bar{\zeta}>0$ and for all $t\geq0$. If the gains are chosen as in (8), it is then possible to show that for any bound $\bar{\zeta}$, there is a large enough L that ensures bounded error trajectories. More importantly, increasing L reduces the ultimate bound of the error. These properties are inherited from the high-gain structure and are summarized in the next theorem, for the presentation of which we introduce the following matrix

$$P=\begin{bmatrix}\frac{h_1}{2h_0}(1+\gamma) & -\frac{1}{2}\\ -\frac{1}{2} & \frac{h_0^2+h_1(1+\gamma)}{2h_0h_1}\end{bmatrix},\tag{10}$$

$$\gamma=\frac{1}{\sqrt{2}h_1}+\frac{h_0^2(\sqrt{2}-1)^2}{\sqrt{2}h_1}.\tag{11}$$

Theorem 2. Consider the error system (7) and assume that $|\zeta(t)|\leq\bar{\zeta}$ for some given constant $\bar{\zeta}>0$ and for all $t\geq t_0\geq0$. Consider the positive definite matrix P given in (10). Design $L>0$, such that

$$\frac{\lambda_{\min}^{1/2}(P)}{2\lambda_{\max}^{3/2}(P)}\geq\frac{\bar{\zeta}}{L^2}.\tag{12}$$

Choose the gains k_p and k_i according to (8). Then, any error trajectory starting at $t_0\geq0$ in $\tilde{x}_0$ satisfying

$$\|\tilde{x}_0-s\|\leq\frac{\lambda_{\min}(P)\min\{\sqrt{2}\pi,4L\}}{8L\lambda_{\max}(P)},s\in\mathcal{S},\tag{13}$$

with $\mathcal{S}$ given in (9), remains bounded and satisfies

$$\|\tilde{x}(t)-s\|\leq d_1\|\tilde{x}_0-s\|\mathrm{e}^{-d_2L(t-t_0)}+\frac{d_3}{L^2}\bar{\zeta},\tag{14}$$

for some positive constants d_i, $i=\{1,2,3\}$.

Proof. See Appendix A.

The anticipated properties of ensuring a region of attraction by a proper selection of L and the attenuation of the disturbance effect, are shown in (12) and (14). These two expressions provide meaningful criteria to choose L given in (8).
An important aspect is the effect of noise or other disturbances in the feedback term $v_q(t)$. It is well known that the use of a high gain amplifies the effect of this class of disturbances (Khalil, 2017, Ch. 8). However, in the PLL setting, the main source of disturbances is not noise, but deviations symmetry model, see Section 2. These deviations are commonly represented as unbalances and harmonics and several methods have been developed to attenuate their effects. Three of the most prominent of these approaches are discussed in the next section.

4. PLL IMPLEMENTATIONS FOR DISTORTED SIGNALS

In practical scenarios, the measured AC signals present deviations from the model (1). In PS, the latter is described using unbalances and harmonics. In an unbalanced signal either the phase shifts between the signal's components differ from $\pm2/3\pi$ or each component has a different magnitude or both (Akagi

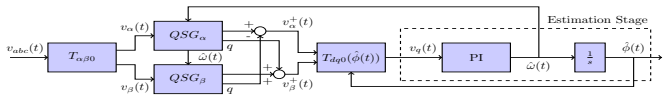

Fig. 2. Block diagram of the DSOGI-PLL.

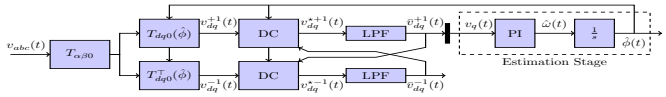

Fig. 3. Block diagram of the DDSRF-PLL.

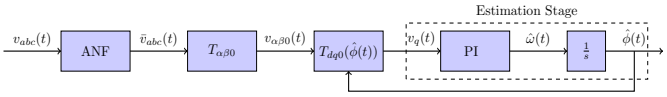

Fig. 4. Block diagram of the ESRF-PLL.

et al., 2007). In the case of harmonics, the measured signal contains a number of additional trigonometric terms, whose frequencies are equal to an integer multiple of the fundamental frequency $\omega(t)$ (Arrillaga and Watson, 2003).

The presence of such distortions breaks the the symmetric model (1) and thus the one of $v_q(t)$ in (3). As a consequence, the estimation quality provided by the SRF-PLL implementation (4) deteriorates. Therefore, different strategies have been proposed to robustify the SRF-PLL implementation (4) (Teodorescu et al., 2011). The general approach is to add a "pre-filtering" stage in order to recover the symmetric structure and thus also the structure of $v_q(t)$ in (3). The resulting "pre-filtered" signal is then fed to the PI control (4). Hence, the dynamics (4) can be regarded as a canonical structure of many popular PLL implementations, which implies that the proposed design criterion in Theorem 2 is applicable to a wide variety of available PLLs.

It is well-known that unbalanced signals can be decomposed into three *sequences*, namely positive, negative and zero sequence, from which the positive and the negative sequences are *symmetric* three-phase AC signals, and where the positive sequence has the same fundamental frequency (Teodorescu et al., 2011). The main idea in PLL applications is thus to extract the positive sequence for its use in the PLL implementation. In the case of harmonics, the standard way of addressing their presence is the use of low-pass filters. More recent methods propose the use of so-called adaptive notch filters (ANF), which are capable of extracting the fundamental component of the signal (Mojiri et al., 2007).

These insights have lead to several PLL variants of which three popular implementations are briefly reviewed below. Then the performance of these different PLLs under heavy distorted conditions and when tuned following Theorem 2 is investigated in Section 5 via simulation.

(1) The dual second order generalized integrator PLL (DSOGI-PLL), introduced in (Rodríguez et al., 2006), addresses the presence of unbalances. The method uses a filter termed *quadrature signal generator* (QSG) with the objective of extracting the *positive sequence* of the input signal from its representation in the $\alpha\beta-$coordinates. The positive sequence is then used in the Park transformation and subsequently in the PI control (4). The authors in Rodríguez et al. (2006) already recognized the problem of changes in the frequency and have proposed to "adapt" the cut-off frequency of the QSG with the estimate obtained from the PI control. The structure of the DSOGI-PLL is described in the block diagram shown in Figure 2.

Table 1. Disturbances considered in the test scenarios.

	Freq. Variation	Unbalances	Harmonics
Scenario 1	•		
Scenario 2	•	•	
Scenario 3	•		•
Scenario 4	•	•	•

Table 2. Amplitude in percentage of the different harmonics.

Number	3	5	7	9	11	13	15	17
Amplitude (%)	6	5	5	1.5	3.5	3	0.5	2

(2) An alternative to the DSOGI-PLL is the decoupled double synchronous reference frame PLL (DDSRF-PLL), proposed in (Rodriguez et al., 2007), which also addresses the presence of unbalances. This implementation applies the Park transformation and its transpose to the measured signal in the $\alpha\beta-$coordinates, and their outputs are used in a *decoupling cell* (DC) with the idea of extracting the positive and negative sequences expressed in the $dq-$coordinates. Then, a low pass filter (LPF) is used to attenuated any residual oscillation introduced by the DC. The outcome of the process is a filtered version of the $q-$component of the positive sequence of the original signal, which is then used as input for the PI control. A block diagram of the DDSRF-PLL is given in Figure 3.

(3) The enhanced synchronous reference frame PLL (ESRF-PLL) (Yazdani and Bakhshai, 2009) addresses the presence of harmonics by filtering the input signal with an ANF. The ANF (Mojiri et al., 2007) estimates a specified number of harmonics by representing each of them with a second order equation and assuming a constant frequency. The estimate of the fundamental harmonic component is then selected as the output of the ANF for its later use in the SRF-PLL (4). The block diagram of the ESRF-PLL is given in Figure 4.

5. PERFORMANCE COMPARISON OF THE DIFFERENT PLL IMPLEMENTATIONS

The tuning criterion proposed in Theorem 2 is applied to the SRF-PLL (4) and the PLL implementations reviewed in Section

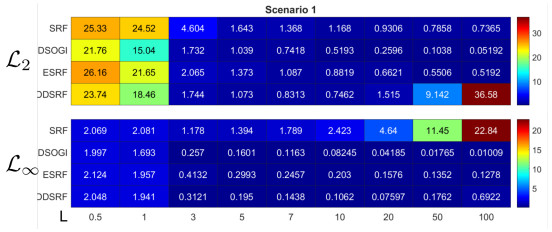

Fig. 5. Frequency estimation error norms in Scenario 1: Only frequency variation is considered.

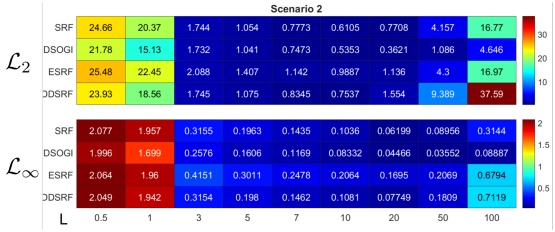

Fig. 6. Frequency estimation error norms in Scenario 2: Frequency variation and unbalances are considered.

4, which we recall all contain the "canonical" implementation (4) in conjunction with some prefiltering stage. The resulting performance is evaluated in a numerical case study. The main objective is to identify which of the estimation methods benefits most from the proposed tuning approach. Thereby, we consider all three sources of perturbation discussed in the paper, i.e., frequency variations, unbalances and harmonics. In total, four scenarios are investigated, which are detailed in Table 1.

For the simulation, the nominal input to the different PLL implementations corresponds to a symmetric three-phase voltage with an amplitude of 220 [V-RMS] and a frequency of 50 [Hz]. The introduced unbalances are an angle deviation of $-15°$ and $10°$ in the components b and c of $v_{abc}(t)$ and a modification of each component's amplitude corresponding to 90%, 105% and 95% of the nominal value. In the case of harmonics, only odd multiples of the base frequency are considered. The considered harmonic components range from one to seventeen. The amplitude of each harmonic is given in Table 2 as a percentage of the nominal signal amplitude. To establish the percentage, the Table 2 in (Markiewicz and Klajn, 2004) was used as guideline. When unbalances and harmonics are present simultaneously, the previous described unbalanced conditions are introduced to each harmonic component. Finally, the frequency variation $\omega(t)=2\pi f(t)$ is generated using the formula

$$f(t)=\begin{cases} 50 & t<10, \\ 50-4\mathbf{e}^{-0.1(t-10)}\sin(0.2(t-10)) & t\geq 10, \end{cases} \text{[Hz]}. \qquad (15)$$

That is, the frequency is constant during the first 10 [s] and then it changes according to the under-frequency profile proposed in (RG-CE System Protection and Dynamics Sub Group, 2018). During the event, the maximum value of the RoCoF is 0.85 [Hz/s] or 5 [rad/s], i.e., $\bar{\zeta}=5$. Finally, it is important to mention that in all cases, the signal was normalized after applying the Clarke transformation.

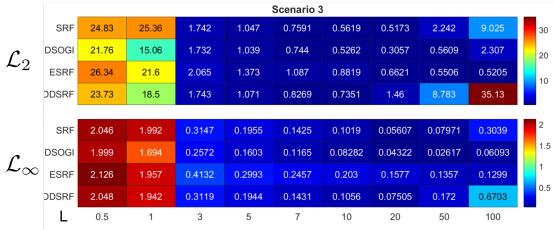

Fig. 7. Frequency estimation error norms in Scenario 3: Frequency variation and harmonics are considered.

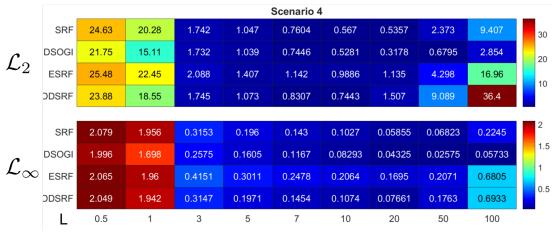

Fig. 8. Frequency estimation error norms in Scenario 4: The three disturbances are present.

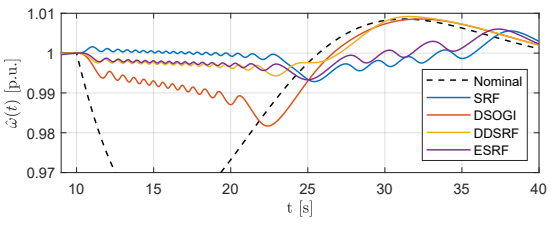

Fig. 9. Estimate of the frequency in Scenario 1 with $L=1$.

In the case of the different PLL implementations, all the PI controllers have the same gains. In all the cases, the gains are chosen following (8) with $h_0=h_1=1$ and L taking the values 0.5, 1, 3, 5, 7, 10, 20, 50 and 100. In the case of the PLL implementations reviewed in Section 4, the following parameters were chosen for the simulation:

(1) For the DSOGI-PLL, the QSG gain in (Rodríguez et al., 2006, Eq. 6) is chosen as $k=1$.

(2) The cut-off frequency of the LPF in the DDSRF-PLL is set to 25 [Hz], following the guideline provided in (Rodriguez et al., 2007, Eq. 11).

(3) The different gains of the ANF in (Yazdani and Bakhshai, 2009, Eq. 4-5) are set to five.

To compare the performance of the implementations, the $\mathcal{L}_2$ and $\mathcal{L}_\infty$ norms of the truncated frequency errors are used. For the norm calculation, only the time interval [10,100] [s] is considered. This is done to avoid including the initial transitory of the estimation. The value of the norms corresponding to the different implementations and scenarios are shown in Figures 5 to 8. The time interval [0,10) [s] in (15) is not only given to allow the estimate to settle down, but to ensure that the estimation error is close to some element of $\mathcal{S}$ before the frequency starts to change. Qualitatively, what can be seen in Figures 5 to 8, is that for $L\geq 3$, both indicators drop drastically. This is associated with the boundedness of the estimation error. In fact, for $L\leq 1$, the implementations are not able of providing an accurate estimate, as is illustrated in Figure 9 for Scenario 1. According to the criterion (12), and for the given parameters, a bounded error is ensured for $L\geq 5.4$, which holds true in all cases. In simulation, error boundedness is also observed for smaller values of L, which given the sufficiency of the criterion (12) is to be expected. The second qualitative behavior observed is the decrease of both norms as L increases. This is associated to the bound (14) and represents the main benefit of the high-gain design, i.e., the attenuation of the RoCoF. However, increasing L in excess results in a deterioration of the metrics because the amplification of unbalances and harmonics overcome the benefit obtained from attenuating the RoCoF. In most of the investigated cases, this happens for $L>20$. It is also worth to mention that in Scenario 4, with all disturbances present, the implementation that accepts the highest gain before showing a decay in the metrics is the DSOGI-PLL, which, at the same time, is the implementation that exhibits the smallest values in both indicators.

Besides the general observations provided above, we would like to remark the following particularities. In Scenario 1 (Figure 5), by increasing L, a deterioration of the $\mathcal{L}_\infty$ norm can be observed in the case of the SRF-PLL. This behavior can be linked to the *peaking phenomenon* associated to high-gain observers (Esfandiari and Khalil, 1992). In Scenario 1 (Figure 5), the $\mathcal{L}_2$ norm deteriorates in the case of the DDSRF-PLL for $L\geq 50$. This happens because the high gain amplifies internal oscillations generated by the DDSRF-PLL. In Scenario 3 (Figure 7), the $\mathcal{L}_2$ norm always decreases by increasing L in the case of the ESRF-PLL. This is linked to the fact that the ESRF-PLL was specifically designed to counteract harmonics. Finally, it is worth to mention that the behavior of the SRF-PLL is quite comparable to the one exhibited by the ESRF-PLL and the DDSRF-PLL, although the SRF-PLL does not include specific mechanisms to counter neither unbalances nor harmonics.

6. CONCLUSIONS

In this work, the SRF-PLL is interpreted as a non-linear high-gain observer that estimates the phase and the frequency of a symmetric three-phase signal. It is shown that, by selecting its gains following a high-gain approach, the effect of the RoCoF can be attenuated. This allows to ensure a robust operation of the SRF-PLL during events of fast frequency changes. It is also recognized that the core structure of the SRF-PLL is present in different PLL implementations, comprising in particular the DSOGI-PLL, DDSRF-PLL and the ESRF-PLL. These implementations include a "pre-filtering" stage aimed at counteracting disturbances like unbalances and harmonics. Therefore, the proposed tuning method also applies to these implementations, and in combination with them, it is possible to use high gain in the presence of distortion. From the reviewed methods, it is observed in simulation that the DSOGI-PLL allows the use of the highest gains without compromising the quality of the estimation. Finally, since the robust stability analysis of the PLL is conducted by means of a strong ISS-Lyapunov function, it is expected that a separation principle between the PLL gain design and standard voltage or current controller designs can be derived. This is of particular interest in the context of frequency support, and will be further investigated in future work.

Appendix A. PROOF OF THEOREM 2

The proof of Theorem 2 consists of three stages. First, a diffeomorphism is introduced in order to obtain a set of new coordinates in which the system dynamics exhibit a linear-like structure. Second, a quadratic ISS-Lyapunov function is derived to obtain bounds on the system trajectories. This step uses some of the ideas in (Besançon, 2007, Theo. 6). Finally, the bounds found in the previous stage are converted back to the original system coordinates.

For the first step, consider the translation $\bar{x}(t) = \tilde{x}(t) - s$, with $s \in \mathcal{S}$ and $\mathcal{S}$ defined in (9). Given the periodicity of (7), the derivative of $\bar{x}(t)$ also satisfies this differential equation. Now, define $z(t) = [z_1(t), z_2(t)]^\top$ and consider the local diffeomorphism

$$\begin{aligned} z_1 &= \frac{1}{2L}\sin\Big(\frac{\bar{x}_1}{2}\Big), \bar{x}_1 \in \Big[-\frac{\pi}{2}, \frac{\pi}{2}\Big], \\ z_2 &= \frac{1}{4L^2}\bar{x}_2, \bar{x}_2 \in \mathbb{R}, \\ \bar{x}_1 &= 2\arcsin\big(2Lz_1\big), z_1 \in \Big[-\frac{1}{2\sqrt{2}L}, \frac{1}{2\sqrt{2}L}\Big], \\ \bar{x}_2 &= 4L^2 z_2, z_2 \in \mathbb{R}. \end{aligned} \tag{A.1}$$

Applying the diffeomorphism (A.1) to the dynamics of $\bar{x}(t)$, one obtains for the dynamics of $z(t)$:

$$\begin{aligned} \dot{z}(t) &= L\alpha(z_1(t))\begin{bmatrix} -h_0\alpha(z_1(t)) & 1 \\ -h_1 & 0 \end{bmatrix} z(t) + \begin{bmatrix} 0 \\ \frac{1}{4L^2} \end{bmatrix}\zeta(t), \\ &= L\alpha(z_1(t))A(z_1(t))z(t) + \frac{1}{4L^2}b\zeta(t), \end{aligned} \tag{A.2}$$

with the function α satisfying

$$\alpha\big(z_1(t)\big) = \sqrt{1-(2Lz_1(t))^2}, \qquad 1 \geq \alpha(z_1(t)) \geq \frac{1}{\sqrt{2}}.$$

For the second stage, and to establish boundedness of solutions of (A.2), let us introduce the quadratic ISS-Lyapunov function candidate

$$\begin{aligned} V(z) &= z^\top P z, \\ \lambda_{\max}(P)\|z\|^2 \geq V(z) &\geq \lambda_{\min}(P)\|z\|^2, \end{aligned} \tag{A.3}$$

where the matrix $P > 0$ is given in (10).

The derivative of V along the trajectories of (A.2) yields

$$\dot{V}(t) = -L\alpha(z_1(t))z^\top(t)Q(z_1(t))z(t) - z^\top(t)Pb\frac{\zeta(t)}{4L^2},$$

where

$$\begin{aligned} Q(z_1(t)) &= -\big(PA(z_1(t)) + A^\top(z_1(t))P\big) \\ &= \begin{bmatrix} h_1\big((1+\gamma)\alpha(z_1(t))-1\big) & \frac{h_0}{2}\big(\alpha(z_1(t))-1\big) \\ \frac{h_0}{2}\big(\alpha(z_1(t))-1\big) & 1 \end{bmatrix}. \end{aligned}$$

Now, for γ as in (11), it can be ensured that $Q(z_1) \geq \frac{1}{2}\mathbf{I}_2$ for all z_1 in its domain of definition, see (A.1). This can be verified by checking that the Schur complement of the difference $Q(z_1) - \frac{1}{2}\mathbf{I}_2$, i.e.,

$$\begin{aligned} \chi_Q &= h_1\Big((1+\gamma)\alpha\big(z_1\big)-1\Big) - \frac{1}{2} - h_0^2\Big(\alpha\big(z_1\big)-1\Big)^2 \\ &\geq h_1\Big(\frac{1+\gamma}{\sqrt{2}}-1\Big) - \frac{1}{2} - h_0^2\Big(1-\frac{1}{\sqrt{2}}\Big)^2, \end{aligned}$$

is positive for γ given in (11). Thus, the time derivative of V can be bounded as

$$\begin{aligned} \dot{V}(t) &\leq -\frac{L}{2\sqrt{2}}\|z(t)\|^2 + z^\top(t)Pb\frac{\zeta(t)}{4L^2} \\ &\leq -\frac{L}{2\sqrt{2}}\|z(t)\|^2 + \frac{1}{4L^2}\|z(t)\|\|Pb\zeta(t)\|. \end{aligned} \tag{A.4}$$

Now, by applying Young's inequality to the positive term in (A.4) and since $\|b\| = 1$, one obtains

$$\frac{1}{4L^2}\|z(t)\|\|Pb\zeta(t)\| \leq \frac{L}{4\sqrt{2}}\|z(t)\|^2 + \frac{\lambda_{\max}^2(P)}{8\sqrt{2}L^5}\bar{\zeta}^2.$$

Using the previous inequality in (A.4), yields

$$\dot{V}(t) \leq -\frac{L}{4\sqrt{2}}\|z(t)\|^2 + \frac{\lambda_{\max}^2(P)}{8\sqrt{2}L^5}\bar{\zeta}^2. \tag{A.5}$$

By accounting for (A.3), (A.5) is transformed into the differential inequality:

$$\dot{V}(t) \leq -\frac{L}{4\sqrt{2}\lambda_{\max}(P)}V(t) + \frac{\lambda_{\max}^2(P)}{8\sqrt{2}L^5}\bar{\zeta}^2. \tag{A.6}$$

In general, it cannot be ensured that the right hand side of (A.6) is non-positive in some region around the origin since the state is bounded and $\bar{\zeta}$ can be arbitrarily large. However, because $\bar{\zeta}$ is divided by L^5, in principle, it is possible to find a suitable large enough value for L that ensures the existence of a positive invariant region for any given $\bar{\zeta}$. This value for L can be determined following a standard high-gain observer approach. To this end, consider the ball centered at the origin

$$\mathcal{B}_1(0) = \Big\{z \in \mathbb{R}^2, \|z\| \leq r = \frac{1}{2\sqrt{2}L}\Big\},$$

and the region inside the maximum level set of V contained in $\mathcal{B}_1(0)$, i.e.,

$$\mathcal{R} = \Big\{z \in \mathbb{R}^2, V(z) \leq \lambda_{\min}(P)r^2 = \frac{\lambda_{\min}(P)}{8L^2}\Big\}. \tag{A.7}$$

A negative semi-definite $\dot{V}(t)$ can be ensured inside $\mathcal{R}$, particularly close to its border, if L is chosen as in (12), meaning that $\mathcal{R}$ in (A.7) is a positive invariant set. Furthermore, the ball

$$\mathcal{B}_2(0) = \Big\{z \in \mathbb{R}^2, \|z\| \leq \frac{\lambda_{\min}(P)}{8\lambda_{\max}(P)L^2}\Big\} \tag{A.8}$$

is included in $\mathcal{R}$, i.e, $\mathcal{B}_2(0) \subset \mathcal{R}$.

Then, accounting for (A.6) and by the application of the Comparison Lemma (Khalil, 2002, Lemma 3.4), for every trajectory starting in $\mathcal{R}$, $V(t)$ satisfies

$$V(t) \leq V(t_0)\mathbf{e}^{-\frac{L}{4\sqrt{2}\lambda_{\max}(P)}(t-t_0)} + \frac{\lambda_{\max}^3(P)}{2L^6}\bar{\zeta}^2.$$

By using (A.3), it follows that

$$\|z(t)\| \leq \sqrt{\frac{\lambda_{\max}(P)}{\lambda_{\min}(P)}}\|z(t_0)\|\mathrm{e}^{-\frac{L(t-t_0)}{8\sqrt{2}\lambda_{\max}(P)}} + \frac{\lambda_{\max}^{3/2}(P)}{\sqrt{2}\lambda_{\min}^{1/2}(P)}\frac{\bar{\zeta}}{L^3}. \quad \text{(A.9)}$$

For the final part, consider again the diffeomorphism (A.1). From the definition of z_1 it follows that

$$\frac{1}{16L^2}\bar{x}_1^2 \geq |z_1|^2 = \frac{\sin^2\left(\frac{\bar{x}_1}{2}\right)}{4L^2} \geq \frac{1}{2\pi^2 L^2}\bar{x}_1^2. \quad \text{(A.10)}$$

By using (A.10), it is possible to bound the norm of z as

$$\frac{\gamma_1}{L}\|\bar{x}\| \geq \|z\| \geq \frac{\gamma_2}{L}\|\bar{x}\|,$$
$$\gamma_1 = \max\left\{\frac{1}{4}, \frac{1}{4L}\right\}, \quad \gamma_2 = \max\left\{\frac{1}{\sqrt{2}\pi}, \frac{1}{4L}\right\}.$$

With the previous bounds, it is possible to ensure that the region described by (13) is mapped inside $\mathcal{B}_2(0)$ in (A.8). Furthermore, (A.9) can be expressed as

$$\|\bar{x}(t)\| \leq \frac{\gamma_1}{\gamma_2}\sqrt{\frac{\lambda_{\max}(P)}{\lambda_{\min}(P)}}\|\bar{x}(t_0)\|\mathrm{e}^{-\frac{L(t-t_0)}{8\sqrt{2}\lambda_{\max}(P)}} + \frac{\lambda_{\max}^{3/2}(P)}{\sqrt{2}\gamma_2\lambda_{\min}^{1/2}(P)}\frac{\bar{\zeta}}{L^2}.$$

Then, Theorem 2 holds with constants

$$d_1 = \frac{\gamma_1}{\gamma_2}\sqrt{\frac{\lambda_{\max}(P)}{\lambda_{\min}(P)}}, \quad d_2 = \frac{1}{8\sqrt{2}\lambda_{\max}(P)}, \quad d_3 = \frac{\lambda_{\max}^{3/2}(P)}{\sqrt{2}\gamma_2\lambda_{\min}^{1/2}(P)}.$$

REFERENCES

Abramovitch, D.Y. (1990). Lyapunov redesign of analog phase-lock loops. *IEEE Trans. Commun.*, 38(12), 2197–2202.

Akagi, H., Watanabe, E.H., and Aredes, M. (2007). *Instantaneous power theory and applications to power conditioning*. IEEE Press and John Wiley & Sons, Hobokem, NJ, USA.

Arrillaga, J. and Watson, N.R. (2003). *Power System Harmonics*. John Wiley & Sons, West Sussex, PO19 8SQ,England.

Besançon, G. (2007). *Nonlinear Observers and Applications*, chapter An Overview on Observer Tools for Nonlinear Systems, 1–33. Springer, Berlin, Heidelberg.

Bizzarri, F., Brambilla, A., and Milano, F. (2018). Analytic and numerical study of TCSC devices: Unveiling the crucial role of phase-locked loops. *IEEE Trans. Circuits Syst. I, Reg. Papers*, 65(6), 1840–1849.

Esfandiari, F. and Khalil, H.K. (1992). Output feedback stabilization of fully linearizable systems. *INT J CONTROL*, 56(5), 1007–1037.

Freijedo, F.D., Doval-Gandoy, J., Lopez, O., and Acha, E. (2009). Tuning of phase-locked loops for power converters under distorted utility conditions. *IEEE Trans. Ind Appl.*, 45(6), 2039–2047.

Göksu, Ö., Teodorescu, R., Bak, C.L., Iov, F., and Kjær, P.C. (2014). Instability of wind turbine converters during current injection to low voltage grid faults and PLL frequency based stability solution. *IEEE Trans. Power Syst.*, 29(4), 1683–1691.

Golestan, S., Monfared, M., and Freijedo, F.D. (2013). Design-oriented study of advanced synchronous reference frame phase-locked loops. *IEEE Trans. Power Electron.*, 28(2), 765–778.

Khalil, H.K. (2002). *Nonlinear Systems*. Prentice Hall, Upper Saddle River, NJ.

Khalil, H.K. (2017). *High-Gain Observers in Nonlinear Feedback Control*. Society for Industrial and Applied Mathematics, Philadelphia, PA.

Khan, S., Bletterie, B., Anta, A., and Gawlik, W. (2018). On small signal frequency stability under virtual inertia and the role of PLLs. *Energies*, 11(9), 2372.

Ma, J., Qiu, Y., Li, Y., Zhang, W., Song, Z., and Thorp, J.S. (2017). Research on the impact of DFIG virtual inertia control on power system small-signal stability considering the phase-locked loop. *IEEE Trans. Power Syst.*, 32(3), 2094–2105.

Markiewicz, H. and Klajn, A. (2004). Standard en 50160 - voltage characteristics in public distribution systems. Technical report, Copper Development Association Inc.

Milano, F., Dörfler, F., Hug, G., Hill, D.J., and Verbič, G. (2018). Foundations and challenges of low-inertia systems. In *2018 PSCC*, 1–25.

Mojiri, M., Karimi-Ghartemani, M., and Bakhshai, A. (2007). Time-domain signal analysis using adaptive notch filter. *IEEE Trans. Signal Process*, 55(1), 85–93.

Ørum, E., Kuivaniemi, M., Laasonen, M., Bruseth, A.I., Jansson, E.A., Danell, A., Elkington, K., and Modig, N. (2015). Future system inertia. Technical report, ENTSOE, Brussels, Tech. Rep.

Poolla, B.K., Groß, D., and Dörfler, F. (2019). Placement and implementation of grid-forming and grid-following virtual inertia and fast frequency response. *IEEE Trans. Power Syst*, 34(4), 3035–3046.

Rantzer, A. (2001). Almost global stability of phase-locked loops. In *40th IEEE CDC*, 899–900.

RG-CE System Protection and Dynamics Sub Group (2018). Rate of change of frequency (RoCoF) withstand capability. Technical report, ENTSO-E. URL `https://docstore.entsoe.eu/Documents/Network\20codes\%20documents/NC\%20RfG/IGD_RoCoF_withstand_capability_final.pdf`.

Rocabert, J., Luna, A., Blaabjerg, F., and Rodriguez, P. (2012). Control of power converters in AC microgrids. *IEEE Trans. Power Electron.*, 27(11), 4734–4749.

Rodríguez, P., Teodorescu, R., Candela, I., Timbus, A.V., Liserre, M., and Blaabjerg, F. (2006). New positive-sequence voltage detector for grid synchronization of power converters under faulty grid conditions. In *37th IEEE PESC*, 1–7.

Rodriguez, P., Pou, J., Bergas, J., Candela, J.I., Burgos, R.P., and Boroyevich, D. (2007). Decoupled double synchronous reference frame pll for power converters control. *IEEE Trans. Power Electron.*, 22(2), 584–592.

Rueda-Escobedo, J.G., Moreno, J.A., and Schiffer, J. (2019). Finite-time estimation of time-varying frequency signals in low-inertia power systems. In *18th ECC*, 2108–2114.

Schiffer, J., Zonetti, D., Ortega, R., Stanković, A.M., Sezi, T., and Raisch, J. (2016). A survey on modeling of microgrids—from fundamental physics to phasors and voltage sources. *Automatica*, 74, 135 – 150.

Teodorescu, R., Liserre, M., and Rodrígez, P. (2011). *Grid converters for photovoltaic and wind power systems*. IEEE-Wiley press, Chichester PO19 8SQ, United Kingdom.

Tielens, P. and Hertem, D.V. (2016). The relevance of inertia in power systems. *Renew. Sustain. Energy Rev.*, 55, 999 – 1009.

Yazdani, D. and Bakhshai, A. (2009). A three-phase harmonic decomposition technique for grid-connected converters. In *2009 IEEE ECCE*, 611–615.